


## RESEARCH ARTICLE

# Age of onset modulates resting-state brain network dynamics in Friedreich Ataxia

Gilles Naeije<sup>1,2</sup>  | Nicolas Coquelet<sup>1</sup> | Vincent Wens<sup>1</sup> | Serge Goldman<sup>1,3</sup> | Massimo Pandolfo<sup>4</sup> | Xavier De Tiège<sup>1,3</sup>

<sup>1</sup>Laboratoire de Cartographie fonctionnelle du Cerveau (LCFC), UNI–ULB Neuroscience Institute, Université libre de Bruxelles (ULB), Brussels, Belgium

<sup>2</sup>Department of Neurology, CUB Hôpital Erasme, Université libre de Bruxelles (ULB), Brussels, Belgium

<sup>3</sup>Department of Functional Neuroimaging, CUB Hôpital Erasme, Université libre de Bruxelles (ULB), Brussels, Belgium

<sup>4</sup>Department of Neurology and Neurosurgery, McGill University, Montreal, Canada

## Correspondence

Gilles Naeije, Laboratoire de Cartographie fonctionnelle du Cerveau (LCFC), UNI–ULB Neuroscience Institute, Université libre de Bruxelles (ULB), Brussels, Belgium.  
Email: gilles.naeije@erasme.ulb.ac.be

## Funding information

Fonds De La Recherche Scientifique - FNRS, Grant/Award Number: J.0095.16.F; Fonds Erasme, Grant/Award Number: Voies du savoir; Friedreich's Ataxia Research Alliance

## Abstract

This magnetoencephalography (MEG) study addresses (i) how Friedreich ataxia (FRDA) affects the sub-second dynamics of resting-state brain networks, (ii) the main determinants of their dynamic alterations, and (iii) how these alterations are linked with FRDA-related changes in resting-state functional brain connectivity (rsFC) over long timescales. For that purpose, 5 min of resting-state MEG activity were recorded in 16 FRDA patients (mean age: 27 years, range: 12–51 years; 10 females) and matched healthy subjects. Transient brain network dynamics was assessed using hidden Markov modeling (HMM). Post hoc median-split, nonparametric permutations and Spearman rank correlations were used for statistics. In FRDA patients, a positive correlation was found between the age of symptoms onset (ASO) and the temporal dynamics of two HMM states involving the posterior default mode network (DMN) and the temporo-parietal junctions (TPJ). FRDA patients with an ASO <11 years presented altered temporal dynamics of those two HMM states compared with FRDA patients with an ASO > 11 years or healthy subjects. The temporal dynamics of the DMN state also correlated with minute-long DMN rsFC. This study demonstrates that ASO is the main determinant of alterations in the sub-second dynamics of posterior associative neocortices in FRDA patients and substantiates a direct link between sub-second network activity and functional brain integration over long timescales.

## KEYWORDS

biomarker, Friedreich ataxia, Hidden Markov modeling, MEG, resting state functional connectivity, resting-state brain network dynamics

## 1 | INTRODUCTION

Friedreich ataxia (FRDA) is the most common autosomal recessive ataxia (Anheim et al., 2010). Most patients are homozygous for the hyper-expansion of an intronic GAA triplet repeat in the frataxin (*FXN*) gene

(Campuzano et al., 1996), which represses *FXN* expression via an epigenetic mechanism (Gottesfeld, 2019). In these patients, most residual *FXN* expression comes from the shorter GAA repeat expansion (*GAA1*), whose length explains 30–50% of the variability in age of symptoms onset and is a determinant of disease severity (Durr et al., 1996; Monterini et al., 1997).

FRDA is characterized by early atrophy of the posterior columns of the spinal cord, followed by progressive degeneration of the

Gilles Naeije and Nicolas Coquelet contributed equally to this work.

This is an open access article under the terms of the Creative Commons Attribution-NonCommercial-NoDerivs License, which permits use and distribution in any medium, provided the original work is properly cited, the use is non-commercial and no modifications or adaptations are made.

© 2021 The Authors. *Human Brain Mapping* published by Wiley Periodicals LLC.

cerebellar dentate nuclei and their efferent fibers in the superior cerebellar pedunculi (Koeppen & Mazurkiewicz, 2013). Clinically, patients become overtly symptomatic only when cerebellar signs appear. Then, variable alterations in pyramidal, visual, auditory and cognitive systems appear over time and contribute to the progression of neurological impairment (Naeije, Rovai, De Tiège, & Pandolfo, 2020; Pandolfo, 2020; Reetz et al., 2018).

The study of resting state (i.e., in the absence of any explicit task) functional connectivity (rsFC) allows to noninvasively characterize the alterations in functional brain architecture in FRDA patients using an experimental paradigm that is free of performance bias. Previous neuroimaging investigations suggested that the level of rsFC is linked with FRDA patients' neurological status. A resting-state functional magnetic resonance imaging (rfMRI) study described that a higher level of rsFC between superior and medial frontal gyri, and angular and cingulate-paracingulate gyri might be associated with better cognitive performances in FRDA patients (Cocozza et al., 2018). Furthermore, a previous magnetoencephalography (MEG) study from our group showed that FRDA patients with symptoms onset after age 12 had significantly higher levels of brain rsFC compared with matched healthy individuals and FRDA patients with symptoms onset before age 12 (Naeije et al., 2020b). These findings suggest that compensatory/adaptive brain mechanisms might slow down FRDA progression, as frequently observed in other degenerative brain disorders such as Alzheimer's disease (AD) (Bobkova & Vorobyov, 2015), Parkinson's disease (PD) (Simioni, Dagher, & Fellows, 2016), and amyotrophic lateral sclerosis (ALS) (Proudfoot et al., 2018), or in acquired brain disorders such as stroke (Park et al., 2011).

The purview of rsFC is however mostly limited to neural integration established over long timescales (i.e., a few minutes), often referred to as “static” rsFC. Thanks to its exquisite, millisecond-scale temporal resolution, MEG offers a unique opportunity to uncover the fleeting dynamics of human brain networks at much finer timescales. Functional couplings among brain networks have been shown to spontaneously fluctuate over a few seconds around a stable backbone of resting-state networks (RSNs) (de Pasquale, Della Penna, Sporns, Romani, & Corbetta, 2016; O'Neill et al., 2015; Wens et al., 2019). Furthermore, the distributed modulations of resting brain network activity emerges as even shorter, sub-second lived “bursts” of electrophysiological activity (Baker et al., 2014; van Ede, Quinn, Woolrich, & Nobre, 2018). The study of this fine network dynamics is efficiently captured by hidden Markov modeling (HMM) of MEG power envelope (i.e., the amplitude variations of ongoing neural oscillatory dynamics) (Brookes et al., 2018). The power envelope HMM identifies transient brain network configurations (referred to as “states” in the HMM terminology) by classifying distinct patterns of power envelope (co)variance consistently repeating in time (O'Neill et al., 2018). From rest MEG data, about 6–8 (or more) (Stevner et al., 2019) transient recurring states lasting 100–200 ms are typically disclosed and show a spatial network topography quite similar to some RSNs (Hawkins et al., 2020; Sitnikova, Hughes, Ahlfors, Woolrich, & Salat, 2018). This approach was already used to demonstrate a link between the

temporal stability of RSN activations and the level of *ZDHHC9* gene expression in subjects with *ZDHHC9* mutations causing X-linked intellectual disability (Hawkins et al., 2020). It was also able to discriminate healthy elders from AD patients, whose spontaneous synchronization in the default mode network (DMN) was less likely and less stable, probably due to a reduction in “static” (i.e., over longer timescales) DMN functional integration that is a core feature of AD (Puttaert et al., 2020; Sitnikova et al., 2018). Although FRDA-related alterations of brain rsFC over long timescales (i.e., minute long) have been previously characterized (Naeije et al., 2020c), data on potential alterations of fast RSNs dynamics are, to the best of our knowledge, not available.

This MEG study, therefore, aims at using HMM to characterize FRDA-related changes in brain network sub-second dynamics, their main determinants, and their relationship with changes in static (i.e., minute-long rsFC) functional brain integration to enhance our understanding of the impact of this multi-system (i.e., spinal, cerebellar and cerebral) disorder on the hierarchy of timescales pertaining to human brain functional architecture. To do so, we used MEG power envelope HMM to compare the fast RSN dynamics between patients with FRDA and matched healthy subjects. Then, we searched for correlations between HMM state temporal parameters (estimating their stability and recurrence) and genetic/clinical parameters (i.e., the size of GAA1 triplet expansion, age of symptoms onset, and the severity of clinical symptoms). Finally, we assessed the link between alterations in HMM state dynamics and static rsFC in patients with FRDA.

## 1.1 | Participants

Fifteen right-handed and one left-handed patients with FRDA, and sixteen healthy individuals matched for age, sex and handedness without any history of neurologic or psychiatric disease were included (Table 1). Of note, two patients with FRDA (and their corresponding healthy subjects) were excluded from the initial cohort of eighteen patients used in previous studies (Marty et al., 2019; Naeije, Wens, et al., 2020b) due to specific methodological issues related to HMM analyses (see Section 2).

All participants contributed to the study after written informed consent and prior approval of the study by the CUB Hôpital Erasme Ethics Committee (Reference EudraCT/CCB: B406201317212).

**TABLE 1** Characteristics of the included patients with FRDA

Age (median, [range], years)	27 [12–51]
SARA (median, [range]/40)	21 [4.5–32]
Age of symptoms onset (median, [range])	11 [4–20]
Disease duration (median, [range], years)	13 [4–38]
GAA1 (median, [range])	638 [280–1,000]

Abbreviations: GAA1, number of GAA1 triplet expansion on the shortest allele; SARA, score on the Scale for the Assessment and Rating of Ataxia.

## 2 | METHODS

### 2.1 | Data acquisition

Neuromagnetic activity was recorded at rest (5 min, eyes opened, fixation cross, online band-pass filter: 0.1–330 Hz, sampling frequency: 1 kHz) with a 306-channel whole-scalp-covering MEG system (Vectorview system, 10 FRDA patients, seven healthy subjects; Triux system, six FRDA patients, eleven healthy subjects; MEGIN, Helsinki, Finland) installed in a lightweight magnetically shielded room (Maxshield, MEGIN, Helsinki, Finland; see (De Tiège et al., 2008) for details). Of note, Vectorview and Triux MEG systems have identical sensor layout (i.e., 102 magnetometers and 102 pairs of orthogonal planar gradiometers) but differ in sensor dynamic range. Previous works from our group mixing recordings from these two systems did not reveal any significant difference related to MEG system in data quality (Marty et al., 2019; Naeije et al., 2019), including rsFC studies (Coquelet et al., 2020; Costers et al., 2020; Naeije, Wens, et al., 2020b).

Four head-tracking coils continuously monitored subjects' head position inside the MEG helmet. The location of the coils and at least 200 head-surface points were determined with respect to anatomical fiducials with an electromagnetic tracker (Fastrak, Polhemus, Colchester, VT).

Participants' high-resolution 3D-T1 weighted cerebral MRI were acquired on a 1.5T MRI scanner (Intera, Philips, The Netherlands).

### 2.2 | Data preprocessing

The signal space separation method was first applied offline to continuous MEG data to reduce external magnetic interferences and correct for head movements (Maxfilter; MEGIN, Helsinki, Finland) (Taulu, Simola, & Kajola, 2005). Then, ocular, cardiac, and system artifacts were visually identified and regressed out from raw MEG signals using an independent component analysis (FastICA algorithm on band-passed [0.1–45 Hz] data, dimension reduction to 30 components, hyperbolic tangent nonlinearity).

### 2.3 | Source reconstruction

Participants' structural brain MRI were anatomically segmented using FreeSurfer (Martinos Center for Biomedical Imaging, MA; Freesurfer, <https://surfer.nmr.mgh.harvard.edu>). MEG and MRI coordinate systems were manually co-registered using anatomical fiducial points for initial estimation and head-surface points to refine the surface co-registration. Then, a 5-mm regular grid of three-dimensional dipole locations was built in the Montreal Neurological Institute (MNI) MRI template and nonlinearly deformed onto each participant's MRI with Statistical Parametric Mapping (SPM12, Wellcome Centre for Neuroimaging, London, UK; <https://www.fil.ion.ucl.ac.uk/spm>). The MEG forward model associated with this source space was finally computed

using the one-layer Boundary Element Method implemented in the MNE-C suite (MNE-C v2.7.3, Martinos Center for Biomedical Imaging, MA; <https://mne.tools/stable/index.html>).

### 2.4 | Hidden Markov modeling of MEG power envelopes

The HMM of MEG source power envelopes was used to investigate FRDA-related alterations in fast brain network dynamics on the whole 5 min of resting state recording of each participant. The methodology was adapted from Coquelet et al. (2020) and Puttaert et al. (2020).

Briefly, cleaned MEG data were wideband filtered (4–30 Hz), then MNE was applied for sources reconstruction using planar gradiometers only (Dale & Sereno, 1993). Of note, we used MNE rather than beamforming for source reconstruction as it has been shown to be a suitable method to image posterior midlines cortices (i.e., precuneus and posterior cingulate cortex) with MEG (Sjögård et al., 2019); these cortices showing significant FRDA-related changes in static functional integration (Naeije, Wens, et al., 2020b). The noise covariance matrix was estimated from 5 min of empty-room data filtered in the same frequency range, and the regularization parameter was fixed according to the consistency condition derived in (Wens et al., 2015). The estimated three-dimensional dipole time series were projected on their direction of maximum variance, and the analytic power envelope of these source signals were then extracted using the Hilbert transform (Wens et al., 2015). The number of transient states ( $K$ ) was set to 6 for consistency with previous MEG envelope HMM studies (Hawkins et al., 2020; Sitnikova et al., 2018; Stevner et al., 2019). The 6-state HMM was inferred from the wide-band (4–30 Hz) source envelope signals, down-sampled at 10 Hz using a moving-window average with 75% overlap (100 ms wide windows, sliding every 25 ms), leading to an effective down-sampling at 40 Hz. Datasets of source envelope signals were demeaned and normalized by the global variance across all sources for each participant, and then temporally concatenated. Group-concatenated envelopes were pre-whitened and reduced to their 40 principal components. The HMM algorithm (Rezek & Roberts, 2005; Woolrich et al., 2013) was then run 10 times (to account for different initial parameters and retain the model with lowest free energy) with a Gaussian observation model using the same model parameters and model selection criteria than in Baker et al. (2014). The Viterbi algorithm (Rezek & Roberts, 2005) was then applied to compute a binary time series of most probable state activation/deactivation. Note that running the group HMM on all patients indicated that two states were driven by only one patient (two different patients for the two states). To ensure that the final HMM was representative of the brain dynamics of all patients with no state driven by one single patient, we thus excluded those two patients (and their corresponding healthy subjects), as previously done in Hunyadi, Woolrich, Quinn, Vidaurre, and De Vos (2019). Importantly, state visits are mutually exclusive, which means that two states cannot be visited simultaneously (Rezek & Roberts, 2005). State power maps, which identify the topography of state-specific power envelope

changes during state activation/inactivation, were computed as the partial correlation between states binary time series and group-concatenated power envelopes (Baker et al., 2014). Those maps were statistically thresholded using a two-tailed parametric correlation tests at  $p < .05$ . The null hypothesis tested was that Fisher-transformed partial correlations follow a Gaussian distribution with mean zero and SD  $\sqrt{1/N_{tdof}-K-2}$ . The number  $N_{tdof}$  of temporal degrees of freedom was estimated as one-quarter of the total number of time samples in group-concatenated envelope signals at 40 Hz sampling frequency, to take into account the 75% overlap in the envelope down-sampling. The critical  $p$ -value was Bonferroni corrected with the number of independent HMM states ( $K-1 = 5$ , due to the constraint that one state is active at any given time) multiplied by the number of spatial degrees of freedom ( $p = 55$ , estimated as the rank for the MEG forward model; see (Wens et al., 2015)). Positive values greater than the significance level were considered as significant and disclosed regions with power increase/decrease upon state activation/inactivation. Negative values below the opposite of the significance level were considered as significant and identified regions with power decrease/increase upon state activation/inactivation. From those topographical maps, we further defined the state power as the partial correlation value averaged over all brain voxels (Brookes et al., 2018). Time series of most probable state activation/inactivation also allowed to extract three temporal parameters that characterized transient brain state dynamics: (i) the mean lifetime (MLT, that is, the mean time spent in each state on a single visit) providing a measure of activation stability, (ii) the fractional occupancy (FO, that is, the fraction of total recording time that the brain spent in each state) that mixes stability and probability of state visit, and (iii) the mean interval length (MIL, that is, mean duration of time intervals of inactive state) providing an inverse measure of state recurrence (Baker et al., 2014; Brookes et al., 2011; Coquelet, Wens et al., 2020; Puttaert et al., 2020).

## 2.5 | Group differences and correlation analyses with HMM state power and temporal parameters

Group-level (i.e., FRDA patients vs. healthy subjects) differences in temporal parameters (i.e., MLT, FO and MIL) and state power were assessed by computing  $F$ -values and derived  $p$ -values using standard nonparametric permutation tests (100,000 random permutations of the group conditions). When performing statistics for the median-split analysis, this aforementioned analysis was completed with post-hoc Tukey's range test. In both cases, significance was set at  $p < .05$  Bonferroni corrected accordingly (see Section 3).

In FRDA patients, HMM states temporal parameters and state power were independently correlated with clinical characteristics (age of symptoms onset, size of GAA1 triplet expansion and SARA score) using Spearman rank correlation. The multiple comparison problem was controlled by Bonferroni correction for the number of clinical scores (i.e., 3) times the number of independent states

(i.e., 5). As it has been previously shown that age of symptoms onset strongly modulates static neuromagnetic rsFC patterns within the FRDA population (Naeije, Wens, et al., 2020b), a post hoc median-split analysis based on age of symptoms onset was further used to contrast dynamic functional brain integration in three groups: FRDA patients with an early age of symptoms onset (i.e., below the median age of symptoms onset), FRDA patients with a late age of symptoms onset (i.e., above the median age of symptoms onset) and healthy subjects. Group-level (i.e., "early" FRDA patients vs. "late" FRDA patients vs. healthy subjects) differences in the temporal parameters and state power of the HMM states that correlated with clinical characteristics were assessed using the same methods as for patients vs. healthy subjects analyses. Significance was set at  $p < .05$  Bonferroni corrected for the number of independent states. A two-tailed Student  $t$ -test was used to compare clinical characteristics of *early* and *late* FRDA patients.

## 2.6 | Link between network temporal stability and functional integration

To get further insights into the relationship between the different timescales of resting-state functional network dynamics, the temporal parameters and state power of the HMM state(s) significantly modulated by FRDA were independently correlated, in patients and healthy subjects, with static rsFC averaged (i.e., *mean network rsFC*, see below) within the network(s) whose state was significantly modulated by FRDA, using Spearman rank correlation. This was done after regressing out power levels of the data to discard possible confounds attributable to power. Significance level was set to  $p < .05$ , Bonferroni corrected for the number of RSNs (i.e., 9) times the number state-related considered (i.e., 2: states 4 and 5) and the number of state parameters (i.e., 4).

Network-level rsFC was computed as in Coquelet, Wens, et al. (2020) and Sjøgård et al. (2020) with the noticeable difference that static power envelope correlation was measured among 155 nodes distributed among 9 well-known RSNs in a developed extension (Naeije, Wens, et al., 2020c) of the connectome used in our previous study to have better brain coverage. This denser connectome was chosen to increase the accuracy of eventual links between HMM derived measures and rsFC (Della Penna, Corbetta, Wens, & de Pasquale, 2019). The RSN were studied in their preferential frequency bands: dorsal attention (DAN), ventral attention (VAN), Somatosensory-motor (SMN), auditory (AUD), control (CON), fronto-parietal (FPN), and language (LAN) networks in the beta band ( $\beta$ , 13–30 Hz); visual (VIS) and default-mode (DMN) networks in the alpha band ( $\alpha$ , 8–12 Hz) (Della Penna et al., 2019). Envelope correlation was computed after pairwise signal orthogonalization (Brookes et al., 2011) and 1 Hz low-pass filtering of power envelopes. Finally, mean network rsFC was estimated as the average rsFC value across all connections within each RSN as in, for example (Sjøgård et al., 2021).

### 3 | RESULTS

#### 3.1 | HMM states topographical maps

Fast resting-state brain network dynamics was inferred from MNE-reconstructed MEG signals across all participants using HMM, which allowed to reduce whole-brain wideband (4–30 Hz) source power envelopes to 6 transient recurrent brain states.

Figure 1 shows the state power maps of the 6 HMM states identified in the participants. Changes in local state power in a brain area parallel changes in power envelopes in the same area when the brain transiently visits that state.

Topographically, states 1 and 3 showed an inverse modulation of power between visual (increased power, state 1; decreased power, state 3) and sensorimotor (decreased power, state 1; increased power, state 3) networks. States 2 and 6 combined an increased power in lateral temporal cortex (left temporal, state 2; right temporal, state 6) and a decreased power at contralateral parietal lobe (right parietal, state 2; left parietal, state 6). State 4 showed decreased power in posterior nodes of the DMN including left and right angular gyri and posterior midline cortices (i.e., precuneus and posterior cingulate cortex). State 5 show increased power at the bilateral temporo-parietal junction (TPJ).

gyri and posterior midline cortices (i.e., precuneus and posterior cingulate cortex). State 5 show increased power at the bilateral temporo-parietal junction (TPJ).

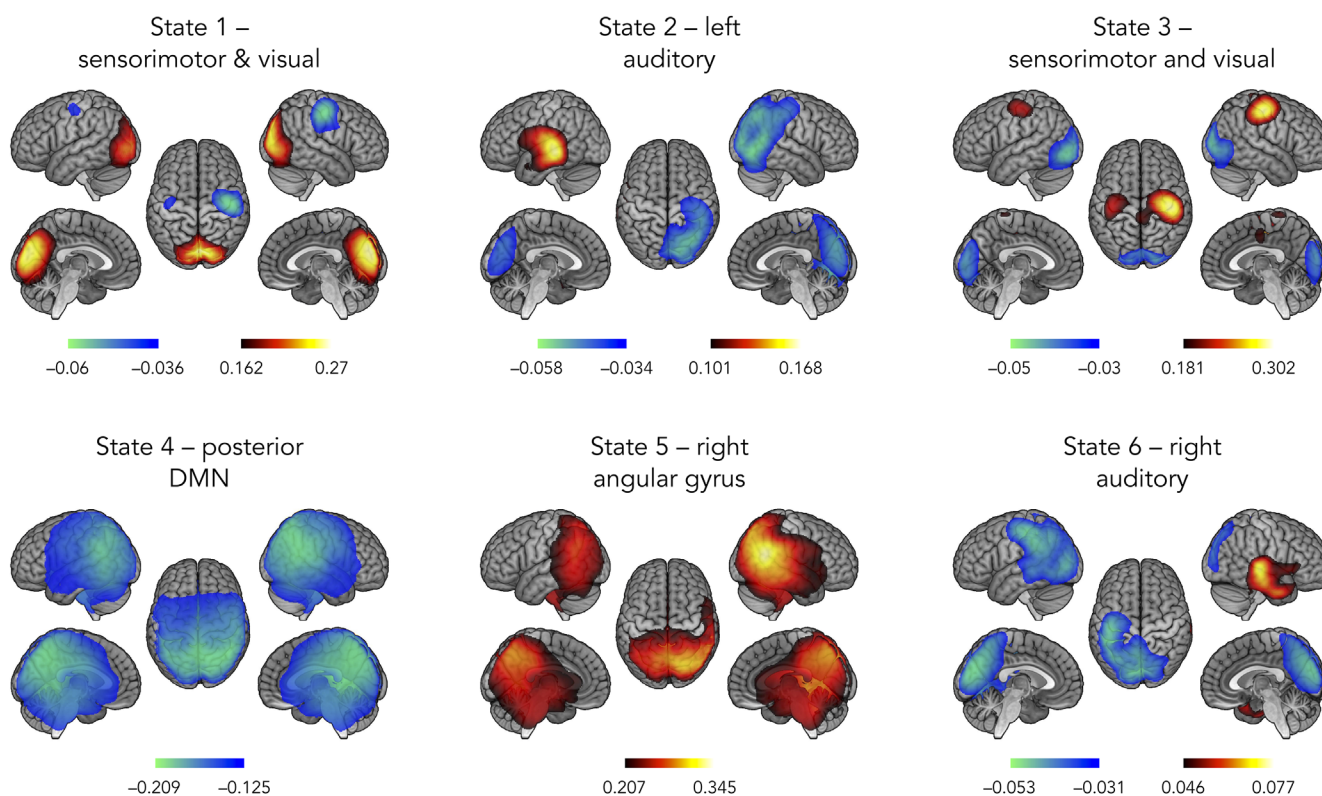
#### 3.2 | Group differences and correlation analyses with HMM state temporal parameters

Figure 2 displays the temporal parameters assessing the transience and stability of each state for each group of participants.

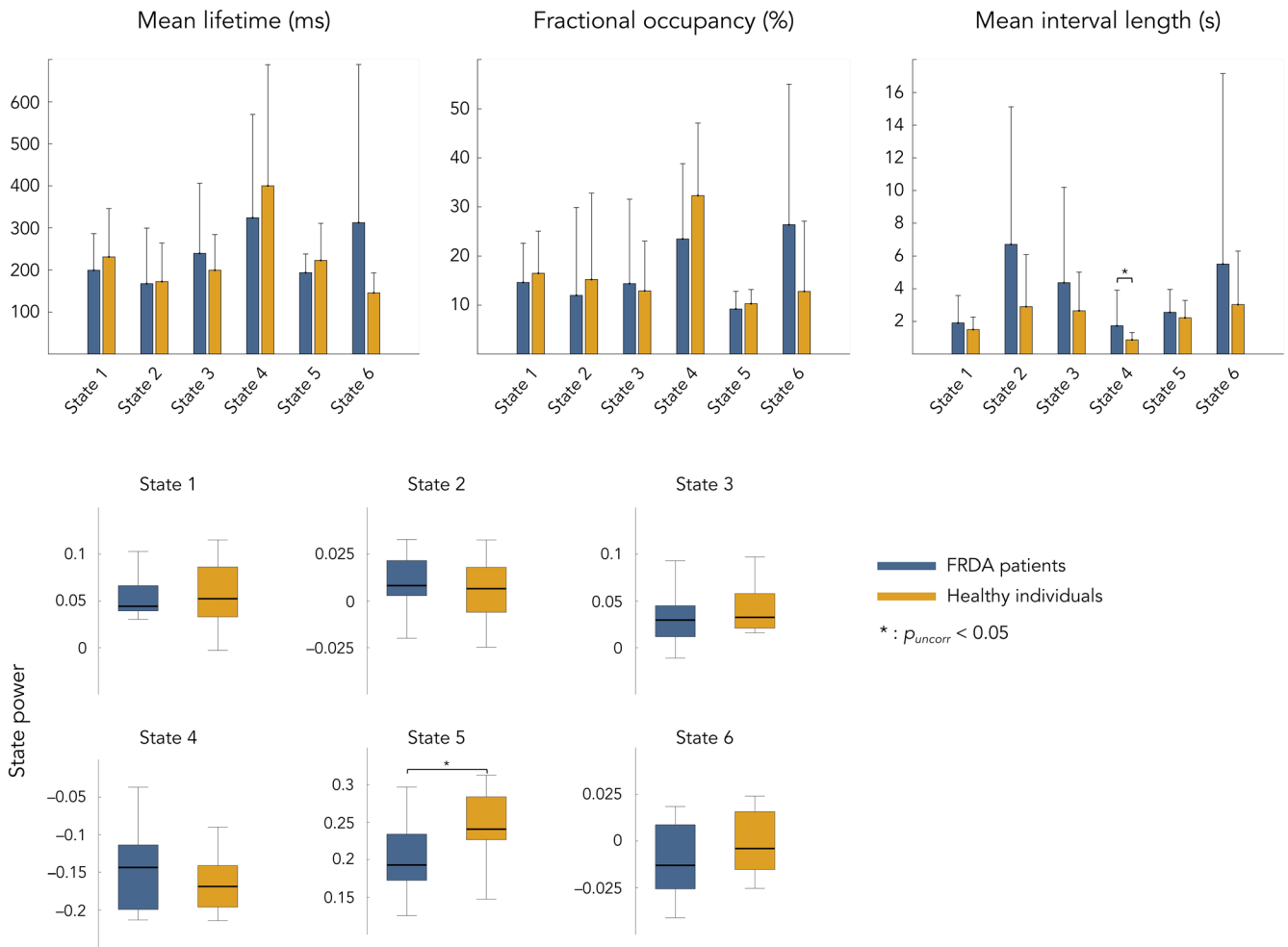
No significant difference between FRDA patients and healthy subjects was found for MLT, FO, MIL and state power of the 6 identified states. MIL of state 4/posterior DMN state tended to be longer in FRDA patients than in healthy subjects, but the difference was not significant after correction for multiple comparisons.

Figure 3 illustrates the results of correlation analyses between state temporal and genetic/clinical parameters in FRDA patients.

Significant positive correlations were found in FRDA patients between the age of symptoms onset and MLT of states



**FIGURE 1** Spatial topographies of the 6 HMM transient states. Red scale refers to the degree of power increase during state visit and blue scale is related to power decrease. These scales are measured in terms of a partial correlation, and as such, have no units. The correlation values have been thresholded between 60% and 100% of the maximum correlation for each state and networks labeled according to the local maxima. Topographically, states 1 and 3 showed an inverse modulation of power between visual (increased power, state 1; decreased power, state 3) and sensorimotor (decreased power, state 1; increased power, state 3) networks. States 2 and 6 combined an increased power in lateral temporal cortex (left temporal, state 2; right temporal, state 6) and a decreased power at contralateral parietal lobe (right parietal, state 2; left parietal, state 6). State 4 showed decreased power in posterior nodes of the DMN including left and right angular gyri and posterior midline cortices (i.e., precuneus and posterior cingulate cortex). State 5 show increased power at the bilateral temporo-parietal junction (TPJ) maximal at the right angular gyrus



**FIGURE 2** Top: Mean and standard error of mean lifetime (left), fractional occupancy (center) and mean interval length (right) associated to each transient state and subjects Bottom: Mean and standard error of state power levels (orange, healthy; dark blue, FRDA). Of notice, power levels values correspond to partial correlation and, as such, have no units. Statistical differences between groups are represented by bars along with  $p$ -value. State numbers and corresponding networks names refer to Figure 1 (state 1 = sensorimotor and visual state; state 2 = left auditory state; state 3 = sensorimotor and visual state; state 4 = posterior DMN state; state 5 = right angular gyrus state; state 6 = right auditory state)

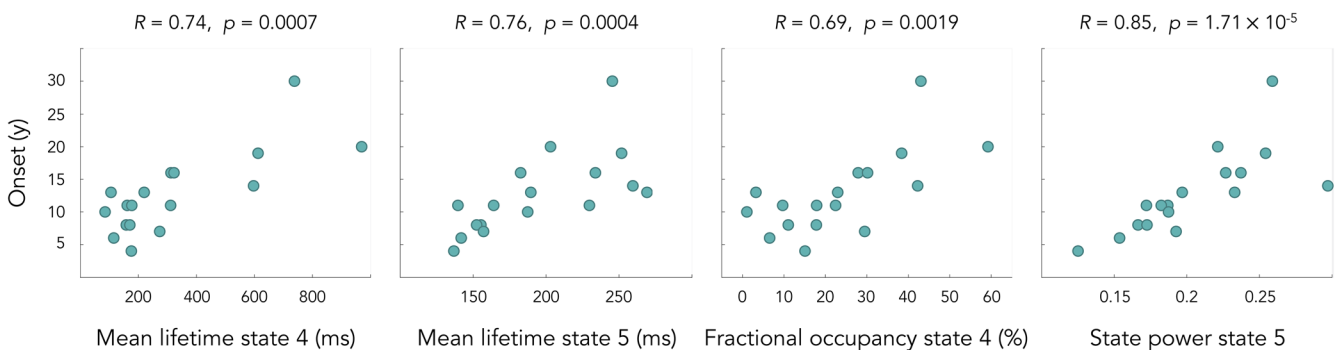


**FIGURE 3** Correlations between age of symptoms onset in years (y) and HMM temporal parameters in FRDA patients. State 4 = posterior DMN state; state 5 = right angular gyrus state

4/posterior DMN state and 5/right angular gyrus state (state 4,  $R = 0.74, p = .0007$ ; state 5,  $R = 0.76, p = .0004$ ), with FO of state 4 ( $R = 0.69, p = .0019$ ), and with state 5 state power

( $R = 0.85, p = .00017$ ). No other correlation was significant with other genetic/clinical parameters (i.e., size of GAA1 triplet expansion, SARA Score).

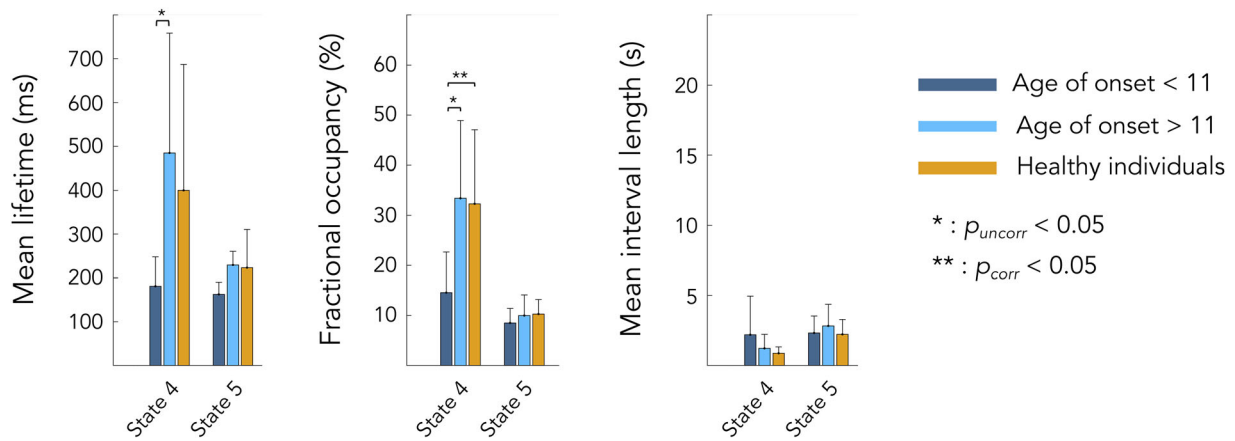


**FIGURE 4** Differences in HMM temporal parameters between healthy participants (orange), FRDA patients with age of symptoms onset <11 years (dark blue) and FRDA patients with age of symptoms onset >11 years (light blue). Statistical differences between groups are represented by bars along with *p*-value. State 4 = posterior DMN state; state 5 = right angular gyrus state

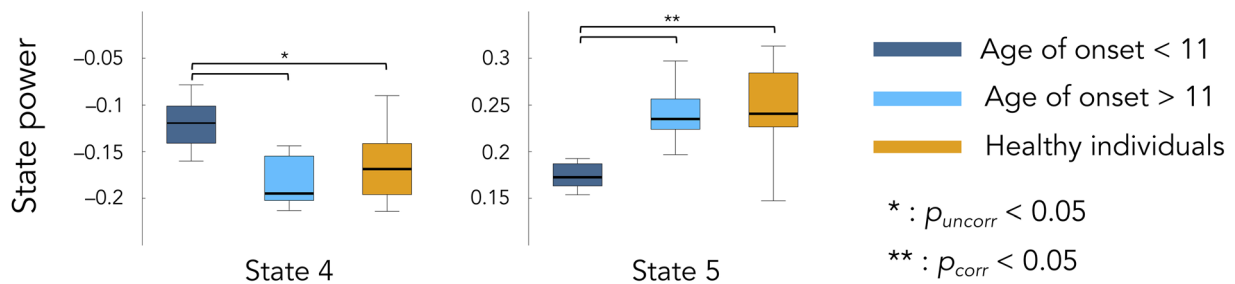


**FIGURE 5** Differences in HMM state powers between healthy individuals (orange), FRDA patients with age of symptoms onset <11 years (dark blue) and FRDA patients with age of symptoms onset >11 years (light blue). Statistical differences between groups are represented by bars along with *p*-value. State 4 = posterior DMN state; state 5 = right angular gyrus state

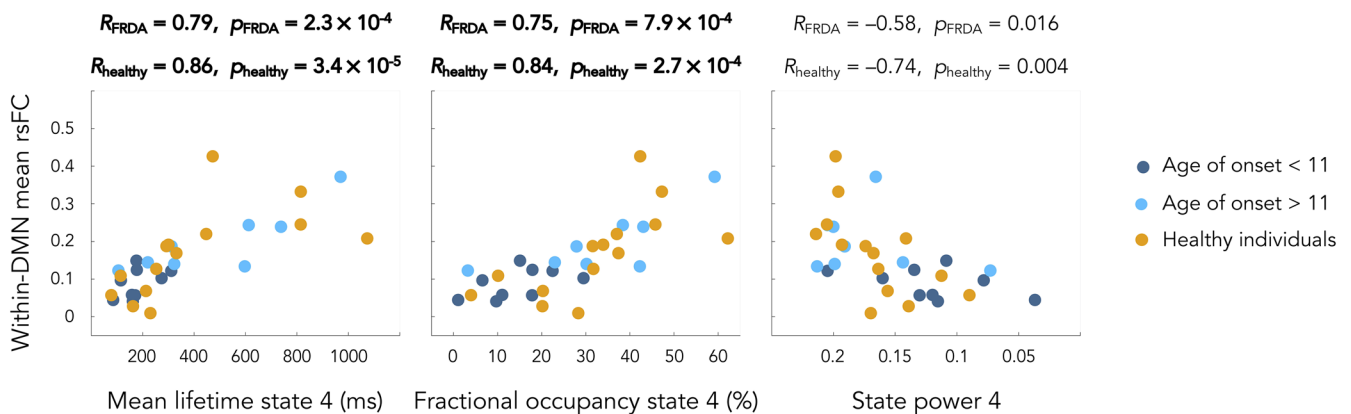


**FIGURE 6** Correlations between mean within DMN static resting state functional connectivity and the temporal parameters of the HMM encompassing the DMN in FRDA patients and healthy individuals. Dark blue dots correspond to FRDA patients with age of symptoms onset <11 years, light blue dots correspond to FRDA patients age of symptoms onset >11 years and orange dots to healthy individuals. Bold text highlights significant correlations. State 4 = posterior DMN state; state 5 = right angular gyrus state

### 3.3 | Median split analysis

Figures 4 and 5 illustrate results of the median split analyses based on the age of symptoms onset for HMM states temporal parameters (Figure 4) and power (Figure 5).

To further characterize the above correlation results revealing a link between posterior DMN dynamics (states 4/posterior DMN state and 5/right angular gyrus) and the age of symptoms onset, we used a post hoc median split on age of symptoms onset by splitting FRDA patients into 2 subgroups based on their age of symptoms onset,

<11 years and > 11 years, similarly to (Harding et al., 2017; Naeije, Wens, et al., 2020b). This median split analysis was used to determine if the transient posterior DMN dynamics of FRDA patients with early/late symptoms onset was different than that of healthy subjects by seeking significant differences in HMM states temporal parameters between these two subgroups and healthy subjects. The median split analysis showed that patients with an age of symptoms onset <11 years old had significantly lower MLT and FO for state 4/posterior DMN state compared to FRDA patients with an onset >11 years (MLT:  $181.1 \pm 66.7$  ms vs.  $484.8 \pm 273.3$  ms,  $p = .048$ ; FO:  $14.6 \pm 8.1$  vs.  $33.4 \pm 15.5$ ,  $p = .02$ ) and healthy subjects (MLT:  $181.1 \pm 66.7$  vs.  $399.9 \pm 287.6$  ms,  $p = .04$ ; FO:  $14.6 \pm 8.1$  vs.  $32.3 \pm 14.8$ ,  $p = .01$ ). Congruently, the magnitude of power decrease (state 4/posterior DMN state) and increase (state 5/right angular gyrus state) upon state visit was lower in patients with an age of symptoms onset <11 years old compared with FRDA patients with an onset >11 years (State 4 power:  $-0.121 \pm 0.045$  vs.  $-0.174 \pm 0.044$ ,  $p = .04$ ; State 5 power:  $0.171 \pm 0.02$  vs.  $0.241 \pm 0.028$ ,  $p = .009$ ) and healthy subjects (State 4 power:  $-0.121 \pm 0.045$  vs.  $-0.166 \pm 0.035$ ,  $p = .04$ ; State 5 power:  $0.171 \pm 0.02$  vs.  $0.248 \pm 0.058$ ,  $p = .001$ ). No other significant difference was observed.

### 3.4 | Link between static and dynamic functional brain integration

To get further insights in patients with FRDA into the relationship between the fast temporal dynamics of the posterior DMN in states 4 (posterior DMN state)/5 (right angular gyrus state) and the corresponding static rsFC of the DMN, we computed the correlation between mean within-DMN static rsFC and the temporal parameters of HMM states 4/5 in patients and healthy subjects. Results are illustrated in Figure 6.

In FRDA patients, significant correlations were found between HMM state 4 MLT and the mean within-DMN rsFC (MLT,  $R = 0.79$ ,  $p = .00023$ ), a strong trend for correlation between HMM state 4 FO and the mean within-DMN rsFC (FO,  $R = 0.75$ ,  $p = .00079$ ) as well as a trend between HMM state 4 and 5 power levels and the mean within-DMN rsFC (State 4 power level,  $R = -0.58$ ,  $p = .016$ ; State 5 power level,  $R = 0.56$ ,  $p = .021$ ). In Healthy subjects, significant correlations were found between HMM state 4 FO, MLT and the mean within-DMN rsFC (FO,  $R = 0.84$ ,  $p = .00027$ ; MLT,  $R = 0.86$ ,  $p = .000034$ ) as well as a trend for correlation between HMM state 5 power levels and the mean within-DMN rsFC ( $R = 0.8$ ,  $p = .001$ ) and between HMM state 4 power levels and the mean within-DMN rsFC ( $R = -0.74$ ,  $p = .004$ ).

## 4 | DISCUSSION

This study shows that the age of symptoms onset in FRDA is related to the fast dynamics of the posterior DMN and the TPJs (henceforth referred to as “posterior associative neocortices”) at rest. Patients with

an early age of symptoms onset (<11 years) visit less often, for shorter duration and with weaker power modulations than patients with a late onset (>11 years), a state of deactivated posterior DMN and spend less time in a state of activated bilateral TPJ. These findings indicate that spontaneous bursts of electrophysiological activity in these posterior associative neocortices is less likely and less stable in FRDA patients with an early onset. This study also demonstrates a direct link in FRDA patients and healthy individuals between static and dynamic functional brain integration within the brain networks comprising these posterior associative neocortices.

The six transient recurrent HMM states occurring in our participants replicated the spatial and temporal patterns of those previously described in healthy individuals and in patients with neurodevelopmental or neurodegenerative disorders (Coquelet, Wens, et al., 2020; Hawkins et al., 2020; Puttaert et al., 2020; Sitnikova et al., 2018; Stevner et al., 2019). Temporal parameters assessing the transience and stability of the six states were strictly in line with previous MEG HMM studies that found MLT varying between 100 and 300 ms, MIL between 2 and 6 s, and an inverse relation between MLT/FO and MIL. Similarly, the FO in our study was within the range usually reported in HMM datasets (Baker et al., 2014; Hawkins et al., 2020; Quinn et al., 2018; Sitnikova et al., 2018). Furthermore, we also identified one particular state (i.e., state 4/posterior DMN state) of deactivated bilateral angular gyri and posterior midline cortices corresponding to a deactivated posterior DMN state. The involvement of posterior midline cortices such as the precuneus and posterior cingulate cortex had not been detected in previous MEG HMM studies performed by other groups (Baker et al., 2014; Brookes et al., 2011; Brookes et al., 2018; Hawkins et al., 2020; Hipp, Hawellek, Corbetta, Siegel, & Engel, 2012; Sitnikova et al., 2018; Stevner et al., 2019), even though they identified similar DMN states. This is presumably related to their use of beamforming for source reconstruction rather than the use of MNE as in this study. Indeed, MNE is better suited to image midline posterior cortices in functional integration studies (Sjøgård et al., 2019), explaining the implication of posterior midline cortices in this HMM states, as previously found by our group both in healthy (Coquelet, Wens, et al., 2020) and pathological (Puttaert et al., 2020) cohorts of participants.

The short-lived states identified by this HMM approach display spatial patterns of neural dynamics that bear some similarity with fMRI- and MEG-derived RSNs (Baker et al., 2014; Biswal, Yetkin, Haughton, & Hyde, 1995; Brookes et al., 2018; de Pasquale et al., 2010). Fast brain dynamics could therefore reflect synchronized neural firing sustained by slower time-scale functional brain connectivity. This potential relationship between functional brain integration occurring over long (i.e., several minutes) and very short (i.e., hundreds of ms) timescales is supported by the correlation between mean DMN rsFC and the fast temporal dynamics parameters and power levels of the HMM states encompassing the posterior DMN. These data are in agreement with studies supporting higher static functional connectivity in the sensorimotor network in relation with increased occupancy of the sensorimotor state (Baker et al., 2014), or increased static rsFC between brain regions as visits to the related state become more



**TABLE 2** Characteristics of FRDA according to the median split based on the age of symptoms onset

Age of symptoms onset (range)	<11 years (4–11 years)	>11 years (12–30 years)	p-value
SARA (median, [range])/40	20.5 [9.5–30.5]	23.5 [4.5–32.5]	.47
GAA1 (median, [range])	877 [680–1,000]	545 [280–835]	.0011
Disease duration (median, [range]; years)	12 [4–38]	13.5 [9–25]	.53

Abbreviations: GAA1, number of GAA1 triplet expansion on the shortest allele; SARA, score on the Scale for the Assessment and Rating of Ataxia.

stable during brain development (Brookes et al., 2018; Coquelet, Wens, et al., 2020).

Age of symptoms onset tightly correlated with the temporal properties of posterior DMN in FRDA. Splitting FRDA patients into two subgroups based on their age of symptoms onset, one with an early (<11 years) and the other with a late (>11 years) age of symptoms onset, disclosed significant differences in the temporal properties and the power levels of the two states involving posterior associative neocortices. Particularly, the state encompassing regions overlapping the posterior DMN showed weaker power modulations and was visited less often and for shorter time intervals in FRDA patients with an early age of symptoms onset compared to FRDA patients with a late onset or healthy subjects. Importantly, FRDA patients with early and late ASO had similar disease duration and SARA score at the time of MEG investigation, but different size of GAA1 triplet expansion (see Table 2). Those two groups of patients therefore mainly differed by the time when they became overtly symptomatic and by their size of GAA1 triplet expansion. In FRDA, the age of symptoms onset relates to the degree of FXN loss, that itself inversely correlates with the size of GAA1 triplet expansion (Campuzano et al., 1997). Pathophysiologically, a decreased expression of FXN involves at the cellular level increased oxidative stress, defective energy production, calcium dyshomeostasis, and impaired mitochondrial biogenesis, leading to mitochondrial dysfunction (Rodríguez-Pascau et al., 2021). Considering that the posterior associative cortices showing altered dynamics in FRDA patients with early age of symptoms onset are parts of the brain regions showing the highest energy consumption at rest (Buckner, Andrews-Hanna, & Schacter, 2008), low FXN levels might particularly impact the neural dynamics of those brain areas during a critical period for brain development leading to sustained impairment in their neural dynamics stability. In patients with a late age of symptoms onset, higher levels of neural FXN expression could still allow the setting of neural dynamics similar to healthy subjects. Still, we failed to find a significant relationship between HMM states temporal parameters/power and the size of GAA1 triplet expansion in our cohort of FRDA patients. The correlation between the size of GAA1 triplet expansion and FXN levels is only partial (Saccà

et al., 2011), GAA1 in peripheral blood cells being only an indirect predictor of FXN expression in the brain (Naeije, Wens, et al., 2020b). So, further longitudinal studies performed in larger cohorts of FRDA patients should investigate the potential link between FXN levels and alterations in brain dynamics at rest.

This study is, limited by the relatively small patient sample. FRDA is a rare disease and MEG is not yet easily accessible for clinical purposes. However, our results are likely to be generally valid as the included patients share the same average characteristics in terms of age, disease duration, SARA score and size of GAA1 triplet expansion as those included in large *clinical cross-sectional* cohorts of FRDA patients (Pandolfo, 2020; Reetz et al., 2015). But, caution is warranted until these findings are validated in a different and larger cohort of patients.

In summary, this MEG study demonstrates that age of symptoms onset is the main determinant of dynamic functional brain integration involving posterior associate neocortices in patients with FRDA. At a more general level, this study provides novel empirical evidence in a pathological human model substantiating a direct link between sub-second and long timescales of human functional brain integration.

## ACKNOWLEDGMENTS

This study was financially supported by the research grant “Les Voies du Savoir” from the Fonds Erasme (Brussels, Belgium), the Fonds de la Recherche Scientifique (FRS-FNRS, Brussels, Belgium; research credit: J.0095.16.F), and a research grant from the Friedreich Ataxia Research Alliance (FARA, Drs Massimo Pandolfo). Xavier De Tiège and Gilles Naeije are Postdoctorate Clinical Master Specialist at the Fonds de la Recherche Scientifique (FRS-FNRS, Brussels, Belgium). The MEG project at the CUB Hôpital Erasme is financially supported by the Fonds Erasme (Research grant “Les Voies du Savoir,” Brussels, Belgium).

## CONFLICT OF INTEREST

None of the authors reports conflicts of interest.

## ETHICS APPROVAL

The study was approved by the CUB Hôpital Erasme Ethics Committee (Reference EudraCT/CCB: B406201317212).

## PATIENT CONSENT

All participants contributed to the study after written informed consent and prior approval of the study by the CUB Hôpital Erasme Ethics Committee.

## DATA AVAILABILITY STATEMENT

Data can be shared upon reasonable request.

## ORCID

Gilles Naeije  <https://orcid.org/0000-0003-1580-1970>

## REFERENCES

- Anheim, M., Fleury, M., Monga, B., Laugel, V., Chaigne, D., Rodier, G., ... Koenig, M. (2010). Epidemiological, clinical, paraclinical and molecular study of a cohort of 102 patients affected with autosomal recessive

- progressive cerebellar ataxia from Alsace, Eastern France: Implications for clinical management. *Neurogenetics*, 11, 1–12. <https://doi.org/10.1007/s10048-009-0196-y>
- Baker, A. P., Brookes, M. J., Rezek, I. A., Smith, S. M., Behrens, T., Probert Smith, P. J., & Woolrich, M. (2014). Fast transient networks in spontaneous human brain activity. *eLife*, 3, e01867. <https://doi.org/10.7554/eLife.01867>
- Biswal, B., Yetkin, F. Z., Haughton, V. M., & Hyde, J. S. (1995). Functional connectivity in the motor cortex of resting human brain using echoplanar MRI. *Magnetic Resonance in Medicine*, 34, 537–541.
- Bobkova, N., & Vorobyov, V. (2015). The brain compensatory mechanisms and Alzheimer's disease progression: A new protective strategy. *Neural Regeneration Research*, 10, 696–697. <https://doi.org/10.4103/1673-5374.156954>
- Brookes, M. J., Groom, M. J., Liuzzi, L., Hill, R. M., Smith, H. J. F., Briley, P. M., ... Liddle, E. B. (2018). Altered temporal stability in dynamic neural networks underlies connectivity changes in neurodevelopment. *NeuroImage*, 174, 563–575.
- Brookes, M. J., Woolrich, M., Luckhoo, H., Price, D., Hale, J. R., Stephenson, M. C., ... Morris, P. G. (2011). Investigating the electrophysiological basis of resting state networks using magnetoencephalography. *Proceedings of the National Academy of Sciences of the United States of America*, 108, 16783–16788.
- Buckner, R. L., Andrews-Hanna, J. R., & Schacter, D. L. (2008). The brain's default network: Anatomy, function, and relevance to disease. *Annals of the New York Academy of Sciences*, 1124, 1–38.
- Campuzano, V., Montermini, L., Lutz, Y., Cova, L., Hindelang, C., Jiralerspong, S., ... Koenig, M. (1997). Frataxin is reduced in Friedreich ataxia patients and is associated with mitochondrial membranes. *Human Molecular Genetics*, 6, 1771–1780.
- Campuzano, V., Montermini, L., Molto, M. D., Pianese, L., Cossee, M., Cavalcanti, F., ... Pandolfo, M. (1996). Friedreich's ataxia: Autosomal recessive disease caused by an intronic GAA triplet repeat expansion. *Science*, 271, 1423–1427.
- Cocozza, S., Costabile, T., Tedeschi, E., Abate, F., Russo, C., Liguori, A., ... Saccà, F. (2018). Cognitive and functional connectivity alterations in Friedreich's ataxia. *Annals of Clinical Translational Neurology*, 5, 677–686.
- Coquelet, N., De Tiège, X., Destoky, F., Roshchupkina, L., Bourguignon, M., Goldman, S., ... Wens, V. (2020). Comparing MEG and high-density EEG for intrinsic functional connectivity mapping. *NeuroImage*, 210, 116556.
- Coquelet, N., Wens, V., Mary, A., Niesen, M., Puttaert, D., Ranzini, M., ... De Tiège, X. (2020). Changes in electrophysiological static and dynamic human brain functional architecture from childhood to late adulthood. *Scientific Reports*, 10, 18986.
- Costers, L., van Schependom, J., Laton, J., Baijot, J., Sjøgård, M., Wens, V., ... Nagels, G. (2020). Spatiotemporal and spectral dynamics of multi-item working memory as revealed by the n-back task using MEG. *Human Brain Mapping*, 41, 2431–2446.
- Dale, A. M., & Sereno, M. I. (1993). Improved localization of cortical activity by combining EEG and MEG with MRI cortical surface reconstruction: A linear approach. *Journal of Cognitive Neuroscience*, 5, 162–176.
- de Pasquale, F., Della Penna, S., Snyder, A. Z., Lewis, C., Mantini, D., Marzetti, L., ... Corbetta, M. (2010). Temporal dynamics of spontaneous MEG activity in brain networks. *Proceedings of the National Academy of Sciences*, 107, 6040–6045.
- de Pasquale, F., Della Penna, S., Sporns, O., Romani, G. L., & Corbetta, M. (2016). A dynamic core network and global efficiency in the resting human brain. *Cerebral Cortex*, 26, 4015–4033.
- De Tiège, X., Op de Beeck, M., Funke, M., Legros, B., Parkkonen, L., Goldman, S., & Van Bogaert, P. (2008). Recording epileptic activity with MEG in a light-weight magnetic shield. *Epilepsy Research*, 82(2–3), 227–231.
- Della Penna, S., Corbetta, M., Wens, V., & de Pasquale, F. (2019). The impact of the geometric correction scheme on MEG functional topology at rest. *Frontiers in Neuroscience*, 13, 1114.
- Durr, A., Cossee, M., Agid, Y., Campuzano, V., Mignard, C., Penet, C., Mandel, J. L., Brice, A., & Koenig, M. (1996). Clinical and genetic abnormalities in patients with Friedreich's ataxia. *The New England Journal of Medicine*, 335(16), 1169–1175.
- Gottesfeld, J. M. (2019). Molecular mechanisms and therapeutics for the GAA-TTC expansion disease Friedreich Ataxia. *Neurotherapeutics*, 16, 1032–1049. <https://doi.org/10.1007/s13311-019-00764-x>
- Harding, I. H., Corben, L. A., Delatycki, M. B., Stagnitti, M. R., Storey, E., Egan, G. F., & Georgiou-Karistianis, N. (2017). Cerebral compensation during motor function in Friedreich ataxia: The IMAGE-FRDA study. *Movement Disorders*, 32, 1221–1229.
- Hawkins, E., Akarca, D., Zhang, M., Brkić, D., Woolrich, M., Baker, K., & Astle, D. (2020). Functional network dynamics in a neurodevelopmental disorder of known genetic origin. *Human Brain Mapping*, 41, 530–544.
- Hipp, J. F., Hawellek, D. J., Corbetta, M., Siegel, M., & Engel, A. K. (2012). Large-scale cortical correlation structure of spontaneous oscillatory activity. *Nature Neuroscience*, 15, 884–890.
- Hunyadi, B., Woolrich, M. W., Quinn, A. J., Vidaurre, D., & De Vos, M. (2019). A dynamic system of brain networks revealed by fast transient EEG fluctuations and their fMRI correlates. *NeuroImage*, 185, 72–82.
- Koeppen, A. H., & Mazurkiewicz, J. E. (2013). Friedreich Ataxia: Neuropathology revised. *Journal of Neuropathology and Experimental Neurology*, 72, 78–90.
- Marty, B., Naeije, G., Bourguignon, M., Wens, V., Jousmäki, V., Lynch, D. R., ... de Tiège, X. (2019). Evidence for genetically determined degeneration of proprioceptive tracts in Friedreich ataxia. *Neurology*, 93, e116–e124.
- Montermini, L., Richeter, A., Morgan, K., Justice, C. M., Julien, D., Castellotti, B., ... Pandolfo, M. (1997). Phenotypic variability in Friedreich ataxia: Role of the associated GAA triplet repeat expansion. *Annals of Neurology*, 41, 675–682. <https://doi.org/10.1002/ana.410410518>
- Naeije, G., Rovai, A., De Tiège, X., & Pandolfo, M. (2020). Hand dexterity and pyramidal dysfunction in Friedreich Ataxia, a finger tapping study. *Movement Disorders Clinical Practice*, 8(1), 85–91.
- Naeije, G., Wens, V., Bourguignon, M., Goldman, S., Pandolfo, M., & de Tiège, X. (2019). Altered neocortical tactile but preserved auditory early change detection responses in Friedreich ataxia. *Clinical Neurophysiology*, 130, 1299–1310. <https://doi.org/10.1016/j.clinph.2019.05.003>
- Naeije, G., Wens, V., Coquelet, N., Sjøgård, M., Goldman, S., Pandolfo, M., & de Tiège, X. P. (2020). Age of onset determines intrinsic functional brain architecture in Friedreich ataxia. *Annals of Clinical Translational Neurology*, 7, 94–104.
- O'Neill, G. C., Bauer, M., Woolrich, M. W., Morris, P. G., Barnes, G. R., & Brookes, M. J. (2015). Dynamic recruitment of resting state sub-networks. *NeuroImage*, 115, 85–95. <https://doi.org/10.1016/j.neuroimage.2015.04.030>
- O'Neill, G. C., Tewarie, P., Vidaurre, D., Liuzzi, L., Woolrich, M. W., & Brookes, M. J. (2018). Dynamics of large-scale electrophysiological networks: A technical review. *NeuroImage*, 180, 559–576.
- Pandolfo, M. (2020). Neurologic outcomes in Friedreich ataxia. *Neurology Genetics*, 6, e415.
- Park, C. H., Chang, W. H., Ohn, S. H., Kim, S. T., Bang, O. Y., Pascual-Leone, A., & Kim, Y. H. (2011). Longitudinal changes of resting-state functional connectivity during motor recovery after stroke. *Stroke*, 42, 1357–1362. <https://doi.org/10.1161/STROKEAHA.110.596155>
- Proudfoot, M., Colclough, G. L., Quinn, A., Wu, J., Talbot, K., Benatar, M., ... Turner, M. R. (2018). Increased cerebral functional connectivity in ALS: A resting-state magnetoencephalography study. *Neurology*, 90, e1418–e1424.

- Puttaert, D., Coquelet, N., Wens, V., Peigneux, P., Fery, P., Rovai, A., ... de Tiège, X. (2020). Alterations in resting-state network dynamics along the Alzheimer's disease continuum. *Scientific Reports*, *10*, 21990.
- Quinn, A. J., Vidaurre, D., Abeysuriya, R., Becker, R., Nobre, A. C., & Woolrich, M. W. (2018). Task-evoked dynamic network analysis through hidden Markov modeling. *Frontiers in Neuroscience*, *12*, 603.
- Reetz, K., Dogan, I., Costa, A. S., Dafotakis, M., Fedosov, K., Giunti, P., ... Schulz, J. B. (2015). Biological and clinical characteristics of the European Friedreich's Ataxia Consortium for Translational Studies (EFACTS) cohort: A cross-sectional analysis of baseline data. *Lancet Neurology*, *14*, 174–182.
- Reetz, K., Dogan, I., Hohenfeld, C., Didszun, C., Giunti, P., Mariotti, C., ... the EFACTS Study Group. (2018). Nonataxia symptoms in Friedreich Ataxia. *Neurology*, *91*, e917–e930. <https://doi.org/10.1212/wnl.0000000000006121>
- Rezek, I., & Roberts, S. (2005). Ensemble hidden Markov models with extended observation densities for biosignal analysis. In *Probabilistic Modeling in Bioinformatics and Medical Informatics* (pp. 419–450). London, England: Springer-Verlag. [https://doi.org/10.1007/1-84628-119-9\\_14](https://doi.org/10.1007/1-84628-119-9_14)
- Rodríguez-Pascual, L., Britti, E., Calap-Quintana, P., Dong, Y. N., Vergara, C., Delaspre, F., ... Pizcueta, P. (2021). PPAR gamma agonist leriglitazone improves frataxin-loss impairments in cellular and animal models of Friedreich Ataxia. *Neurobiology of Disease*, *148*, 105162.
- Saccà, F., Puorro, G., Antenora, A., Marsili, A., Denaro, A., Piro, R., ... Filla, A. (2011). A combined nucleic acid and protein analysis in Friedreich ataxia: Implications for diagnosis, pathogenesis and clinical trial design. *PLoS One*, *6*, e17627.
- Simioni, A. C., Dagher, A., & Fellows, L. K. (2016). Compensatory striatal-cerebellar connectivity in mild-moderate Parkinson's disease. *NeuroImage Clinical*, *10*, 54–62. <https://doi.org/10.1016/j.nicl.2015.11.005>
- Sitnikova, T. A., Hughes, J. W., Ahlfors, S. P., Woolrich, M. W., & Salat, D. H. (2018). Short timescale abnormalities in the states of spontaneous synchrony in the functional neural networks in Alzheimer's disease. *NeuroImage Clinical*, *20*, 128–152.
- Sjøgård, M., de Tiège, X., Mary, A., Peigneux, P., Goldman, S., Nagels, G., ... Wens, V. (2019). Do the posterior midline cortices belong to the electrophysiological default-mode network? *NeuroImage*, *200*, 221–230.
- Sjøgård, M., Wens, V., van Schependom, J., Costers, L., D'hooghe, M., D'haeseleer, M., ... de Tiège, X. (2020). Brain dysconnectivity relates to disability and cognitive impairment in multiple sclerosis. *Human Brain Mapping*, *42*, 626–643. <https://doi.org/10.1002/hbm.25247>
- Stevner, A. B. A., Vidaurre, D., Cabral, J., Rapuano, K., Nielsen, S. F. V., Tagliazucchi, E., ... Kringelbach, M. L. (2019). Discovery of key whole-brain transitions and dynamics during human wakefulness and non-REM sleep. *Nature Communications*, *10*, 1035.
- Taulu, S., Simola, J., & Kajola, M. (2005). Applications of the signal space separation method. *Signal Processing IEEE*, *53*(9), 3359–3372. <https://doi.org/10.1109/TSP.2005.853302>
- van Ede, F., Quinn, A. J., Woolrich, M. W., & Nobre, A. C. (2018). Neural oscillations: Sustained rhythms or transient burst-events? *Trends in Neurosciences*, *41*, 415–417.
- Wens, V., Bourguignon, M., Vander Ghinst, M., Mary, A., Marty, B., Coquelet, N., ... De Tiège, X. (2019). Synchrony, metastability, dynamic integration, and competition in the spontaneous functional connectivity of the human brain. *NeuroImage*, *199*, 313–324.
- Wens, V., Marty, B., Mary, A., Bourguignon, M., op de Beeck, M., Goldman, S., ... De Tiège, X. (2015). A geometric correction scheme for spatial leakage effects in MEG/EEG seed-based functional connectivity mapping. *Human Brain Mapping*, *36*, 4604–4621.
- Woolrich, M. W., Baker, A., Luckhoo, H., Mohseni, H., Barnes, G., Brookes, M., & Rezek, I. (2013). Dynamic state allocation for MEG source reconstruction. *NeuroImage*, *77*, 77–92. <https://doi.org/10.1016/j.neuroimage.2013.03.036>

**How to cite this article:** Naeije, G., Coquelet, N., Wens, V., Goldman, S., Pandolfo, M., & De Tiège, X. (2021). Age of onset modulates resting-state brain network dynamics in Friedreich Ataxia. *Human Brain Mapping*, *42*(16), 5334–5344. <https://doi.org/10.1002/hbm.25621>